Science of the Total Environment 651 (2019) 2830–2844

Contents lists available at ScienceDirect

Science of the Total Environment

journal homepage: www.elsevier.com/locate/scitotenv

Exposure to naphthenic acids and the acid extractable organic fraction from oil sands process-affected water alters the subcellular structure and dynamics of plant cells

Mitchell E. Alberts, Gordon Chua, Douglas G. Muench *

Department of Biological Sciences, University of Calgary, Canada

HIGHLIGHTS

- Plant epidermal cells were exposed to NAs and AEOs
- Microtubule and actin disruption occurred after acute NA and AEO exposure
- Reduced organelle movement and changes in organelle morphology were observed
- ROS levels increased and reduced cell viability was apparent after AEO treatment
- Cellular responses can be used to monitor AEO toxicity and remediation

GRAPHICAL ABSTRACT

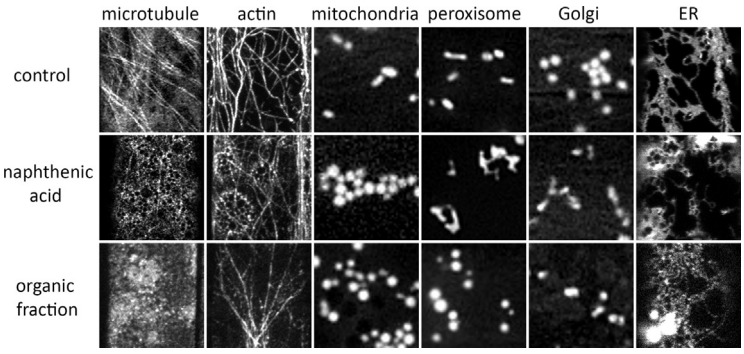

ARTICLE INFO

Article history:
Received 19 July 2018
Received in revised form 12 October 2018
Accepted 12 October 2018
Available online 15 October 2018

Editor: Charlotte Poschenrieder

Keywords:
Oil sands process-affected water
Naphthenic acids
Subcellular responses
Fluorescence microscopy
Cellular biosensor
Reactive oxygen species

ABSTRACT

Oil sands surface mining generates vast quantities of oil sands process-affected water (OSPW) as a by-product of bitumen extraction. The acid extractable organic (AEO) fraction of OSPW contains several contaminants, including naphthenic acids (NAs). While responses of living organisms to NA and AEO exposure have been described at the developmental, physiological, metabolic and gene expression levels, the effects of these compounds at the cellular and subcellular level are limited. Using live cell fluorescence microscopy and a suite of fluorescent marker proteins, we studied the intracellular responses of the plant cell cytoskeleton and several membrane-bound organelles to NA and AEO treatments. A rapid disassembly of cortical microtubules and a decrease in dynamics associated with actin filaments was observed in response to these treatments. Concomitantly, the integrity and dynamics of mitochondria, peroxisomes, Golgi stacks, and endoplasmic reticulum were also altered. AEO treatments were the most toxic to cells and resulted in the accumulation reactive oxygen species. This study provides foundational evidence for intracellular responses to NA and AEO exposure using two evolutionarily diverse model plant cell types. This cellular assay could be used to identify the most toxic components of AEO subfractions, and assist in determining the effectiveness of OSPW remediation efforts.

© 2018 Elsevier B.V. All rights reserved.

1. Introduction

The oil sands region in northern Alberta, Canada contains the third largest oil reserve in the world, covering a total area of 142,000 km^2 and containing an estimated 166 billion barrels of recoverable bitumen

* Corresponding author at: University of Calgary, 2500 University Dr. NW, Calgary, Alberta T2N1N4, Canada.
E-mail address: dmuench@ucalgary.ca (D.G. Muench).

https://doi.org/10.1016/j.scitotenv.2018.10.181
0048-9697/© 2018 Elsevier B.V. All rights reserved.

(CAPP, 2015). Surface mining of oil sands utilizes a hot water extraction process that results in large volumes of oil sands process-affected water (OSPW) that must be stored on-site due to its acute and chronic toxicity to living organisms (Clemente and Fedorak, 2005; Giesy et al., 2010). Clay, sand, salts, heavy metals, residual bitumen, and a wide range of organic and inorganic chemical compounds are present in OSPW (Allen, 2008). The organic fraction (often isolated as acid extractable organics; AEOs) contains a group of toxic compounds referred to as naphthenic acids (NAs). Classically, NAs are defined as carboxylic acids that fit the formula $C_nH_{2n+Z}O_2$, where "n" indicates the number of carbon atoms and "Z" is the hydrogen deficit due to ring cyclization (Whitby, 2010). The occurrence of NAs in crude oil results from the degradation of petroleum-based hydrocarbons, and their concentrations can range between 20 and 130 mg/L in OSPW (Holowenko et al., 2002; Allen, 2008; Grewer et al., 2010). While the AEO fraction contains many classically defined NA types, it also contains other organic compounds that could contribute to its toxicity. These include, but are not limited to, oxy-naphthenic acids (NAs containing more than two oxygen atoms), BTEX (benzene, toluene, ethylbenzene, and xylene), sulfur- and nitrogen-containing compounds, diluents, and other petroleum-based hydrocarbons (Grewer et al., 2010; Bauer et al., 2015; Small et al., 2015; Morandi et al., 2015).

A range of aquatic and terrestrial species have been examined to determine how NA and AEO exposure impacts model biological systems. These have included toxicological studies on bacteria, invertebrates, fish, birds, amphibians and mammals (reviewed in Li et al., 2017). Whole OSPW, organic extracts of OSPW, and purified NAs were shown to have detrimental effects on the development, physiology, reproduction and behavior of test organisms. At the cellular level, these compounds altered gene expression, immunological function and metabolism, and were shown to induce oxidative stress (Li et al., 2017). The toxicity of OSPW on cell proliferation and viability of cultured macrophages has also provided insight into the effects of OSPW and NAs on cell function (Fu et al., 2017). Several studies have examined the toxicological effects of OSPW, NAs and the AEO fraction on aquatic and terrestrial plant species. Fresh weight gains and water uptake of three aquatic plant species common in Alberta (common reed, cattail, and bulrush) were significantly reduced upon treatment of NAs in their non-ionized form (Armstrong et al., 2009). Studies on native plant species have shown that OSPW and commercial NAs also affect water relations and gas exchange (Crowe et al., 2001; Kamaluddin and Zwiazek, 2002; Apostol et al., 2004). Additionally, a study using the model plant species *Arabidopsis thaliana* (Arabidopsis) showed impaired seedling primary root growth and seed germination after NA and AEO exposure (Leishman et al., 2013). Plant-based mRNA profiling has also provided insight into changes in gene expression after AEO exposure. Genes encoding enzymes involved in xenobiotic detoxification and oxidative stress were upregulated in both root and shoot tissue after short term exposure to the AEO fraction (Widdup et al., 2015).

The effects of NA and AEO exposure on the intracellular organization and dynamics of cells has not been studied in detail. Narcosis, the non-specific disruption of membranes through insertion of hydrophobic compounds into the lipid bilayer, has been proposed as a potential mechanism of NA toxicity due to their lipophilic nature (Frank et al., 2008). Evidence supporting NA induced membrane disruption has been observed in rainbow trout hepatocytes, as indicated by a decrease in membrane integrity after exposure to synthetic NAs (Tollefsen et al., 2012). In plants, evidence of increased membrane permeability has been observed in root cells after NA exposure (Pavlović et al., 2015). Disruption of the cell membrane could lead to an influx of NAs and interruption of cellular homeostasis that is essential for proper cellular physiology and development. Here we describe the effects of NAs and the AEO fraction on the subcellular structure, organization and dynamics of plant cells. Using a suite of fluorescent organelle and cytoskeletal markers along with live cell fluorescence microscopy, we aimed to identify the responses of the cytoskeleton and several membrane-bound organelles to these treatments. Arabidopsis and onion epidermal layers were used in this study, and represent model systems from two evolutionarily divergent plant lineages.

2. Materials and methods

2.1. OSPW, NA, and AEO

OSPW was collected from an oil sands mine site located in the Athabasca region of northern Alberta, Canada, and extraction of the AEO fraction was performed using a dichloromethane liquid-liquid acid extraction procedure as previously described (Holowenko et al., 2002). The resulting AEO fraction yield was approximately 70 mg of AEO per litre of OSPW. The AEOs were resuspended in dimethyl sulfoxide (DMSO) at a concentration of 70 mg/mL and stored at room temperature in the dark.

Three NA solutions were also prepared. The first was a mixture of three different single ring (SR) surrogate NAs. These were cyclohexane propionic acid (3-cyclohexylpropionic acid, MW = 156), cyclohexane butyric acid (4-cyclohexylbutanoic acid, MW = 170), and cyclohexane pentanoic acid (3-cyclohexylpentanoic acid, MW = 184, Sigma-Aldrich) suspended in DMSO in equal parts to produce a stock concentration of 100 mg/mL. The second NA solution contained decahydronaphthalene-2-carboxylic acid (DH, MW = 182, a gift from Brian Keay, University of Calgary), a surrogate two-ring NA. The third was 1-adamantanecarboxylic acid (AdCA, MW = 180, Sigma-Aldrich), a model diamondoid NA that was empirically shown to be present in OSPW (Rowland et al., 2011). DH and AdCA were each suspended in DMSO at a stock concentration of 100 mg/mL. Control treatments contained an equivalent concentration of the DMSO carrier.

Working solutions containing either NA or the AEO fraction were prepared in ddH_2O at 10, 25, 50, and 75 mg/L, buffered with 10 mM MES, and adjusted to pH 5.0. The pH of the medium was set at 5.0 because NAs are predominantly in their non-ionized state and are most toxic to plants at low pH (Armstrong et al., 2009; Leishman et al., 2013), and the pH in the microenvironment of the root surface is often lower than the surrounding soil (Rudolph-Mohr et al., 2014). Due to the complex nature of organic species in the AEO fraction, it was not possible to determine molar concentration of the AEO solution. Thus, AEO (and NA) concentrations were measured as weight per volume units, as is commonly reported in NA toxicity studies. Molar concentration conversions (at 50 mg/L) for the purified NAs were 294 μM, 275 μM and 278 μM for SR (mean molarity), DH and AdCA, respectively. Solutions were filter sterilized using Acrodisc 25 mm syringe filters with a pore size of 0.45 μm (Pall Corporation, Ann Arbor, MI) into sterilized flasks and stored at 4 °C in the dark. The concentration of compounds used in this study was within the range of the total AEO concentration found in OSPW (10 to 100 mg/L).

2.2. Organelle and cytoskeletal fluorescent protein markers

Organelle and cytoskeletal fluorescent protein marker plasmids for transient expression in onion epidermal cells were obtained for six plant cell organelles and cytoskeletal components (summarized in Supplemental Table 1). Additionally, Arabidopsis lines stably expressing the six fluorescent protein markers for organelles and cytoskeletal components were used (summarized in Supplemental Table 2).

2.3. Biolistic transfection of onion epidermal cells

Biolistic transfection was used for transient expression of fluorescent protein fusion markers in onion (*Allium cepa* L.) epidermal cells (Scott et al., 1999; Chuong et al., 2005). Plasmid DNA encoding the fluorescent proteins was purified using a plasmid DNA Midiprep kit (Qiagen, Toronto, ON, Canada). Gold particles (1 μm diameter) were coated with 5–10 μg of plasmid DNA and subsequently bombarded into the abaxial

surface of the onion bulb scale segment (1 cm^2) at a pressure of 1100 psi. For the simultaneous expression of two fluorescent markers, 5–10 μg of each marker was mixed together prior to coating gold particles. Following bombardment, onion scale segments were placed abaxial side down on ddH_2O soaked filter paper in a petri dish, sealed with parafilm, and incubated for approximately 16 h at room temperature in a dark environment.

2.4. Seedling growth conditions

Seedlings were grown on plates containing 0.5× Murashige and Skoog medium, 1% sucrose and 0.7% phytoagar adjusted to pH 5.7. Seeds were surface sterilized using two consecutive washes of 70% ethanol for 10 and 5 min, respectively. Surface sterilized seeds were placed linearly on the plates and stratified at 4 °C in the dark for two days. The seeded plates were then placed vertically in a growth chamber set to 16:8 h light:dark cycle for 7–14 days.

2.5. Onion epidermal peel and Arabidopsis seedling treatments

Transiently expressing onion epidermal layers were peeled off the adaxial surface of onion scale segments using forceps and floated on 2 mL of control, NA or AEO solution in 12-well microtitre plates. Similarly, Arabidopsis seedlings were placed on the surface of these solutions with the roots submerged. Mixing of the solution was achieved by gentle orbital shaking of the plates (~40 rpm). Oryzalin (a microtubule depolymerizing drug; Crescent Chemical Co., Inc., NY) was used at a concentration of 5 or 10 μM, latrunculin B (an actin filament depolymerizing drug; Calbiochem, Germany) was used at a concentration of 1 μM.

2.6. Microscopy

Onion epidermal peels and Arabidopsis seedlings were mounted on microscope slides in the corresponding control, NA, or AEO solution. Epifluorescence microscopy was performed using the GFP (480/30 ex; 535/40 em) or mCherry (540/25 ex; 605/55 em) filter sets (Leica DMR). Images were captured using a cooled CCD camera (Retica 1350 EX, QImaging, Surrey, BC, Canada) and exported in the TIFF file format for further processing using ImageJ (v. 1.50 g; Schindelin et al., 2012). Laser scanning confocal microscopy (Leica, TCS-SP5) was performed for GFP detection in Arabidopsis seedlings using an imaging beam strength of 7–20% and gain that was adjusted to 10% (increased if the sample fluorescence was low). The excitation filter was set at 488 nm and the collection range was 508–530 nm.

For microtubule density measurements, a 256 μm^2 area was selected from two regions of each cell that contained microtubules. The sum of microtubule lengths was divided by the measured area to determine microtubule density. A total of 10 cells were used to calculate the mean microtubule density for each treatment. Actin filament density measurements were adapted from a previously described protocol by Higaki et al. (2010). Two 64 μm^2 areas containing actin filaments were selected from each cell for quantification. A threshold was applied to the image, transforming all pixels representing actin filaments white and all background pixels black. The binary images were skeletonized to reduce actin filaments to one pixel in width. Percent density was calculated by dividing the number of white pixels (representing actin filaments) by the total number of pixels in the area, then multiplied by 100. Data was converted to relative values for comparison across different concentrations. A total of 10 cells were used to calculate the mean actin filament density for each treatment.

To determine organelle velocities, image sequences were captured at one frame per second over a 10 s period in NA and AEO treated cells. The ImageJ plug-in MTrackJ (Meijering et al., 2012) was used to manually track individual organelles. Paths of ten organelles that showed the highest velocity in each cell were tracked, and a total of ten cells were used in measurements for each treatment. Mean maximal velocity values were calculated by averaging all instantaneous velocity measurements over the 10 s period for each organelle type and treatment. To determine whether microtubules and Golgi stacks could recover to their normal state after removal of the treatment compound, a 1 hour wash-out period was performed following a 4 h treatment by floating the epidermal peels on 10 mM MES solution (pH 5.0).

Endoplasmic reticulum tubule length was determined by selecting regions measuring 482.4 μm^2 at random from onion epidermal cell images, and the sum of the lengths of all tubules within the selected region was measured. Mean tubule length was calculated by adding the tubule lengths within the selected region and dividing by the total number of tubules. A total of 5 cells were used to quantify mean tubule length for each NA and AEO treatment.

2.7. Onion epidermal cell viability assays

Propidium iodide was used to quantify cell viability after NA and AEO exposure. Onion epidermal cells were exposed to 50 mg/L NA or AEO solution for 4 h and transferred to a solution containing 10 μg/mL propidium iodide for 30 min. The cells were mounted on a slide and imaged by epifluorescence microscopy with the TRITC filter set. Approximately 100 cells were imaged at random for each NA or AEO exposure from 3 to 4 onion epidermal peels, and nuclear staining of cells indicated cell death.

2.8. Determination of H_2O_2 levels

Measurement of AEO-induced reactive oxygen species (ROS) production was performed using Arabidopsis seedlings expressing the H_2O_2 biosensor roGFP2-Orp1 (Scuffi et al., 2018). Seedlings were grown on 0.5× MS (pH 5.7) plates for 10 days as described above. Root hairs were imaged using epifluorescence microscopy directly on the agar plate to reduce potential sources of stress. The tips of individual root hairs were rapidly imaged at the initial moment of root hair selection and 10 min after treatment was initiated. A 63× long working distance water immersion lens was used for imaging with a UV filter set (340–380 ex; 425 LP em) and the blue (eGFP) filter set (480/30 ex; 535/40 em). The fluorescence of the roGFP2-Orp1 biosensor was imaged sequentially using the UV and blue filter sets. The seedling immersion solutions consisted of a DMSO control, 100 mg/L AEO, or 10 mM H_2O_2 in liquid 0.5× MS medium (pH 5.7). Roots hairs from the mid-region of the primary root were treated with a bead of liquid medium suspended between the objective lens and the root on the surface of the plate. The H_2O_2 treatment was used to induce oxidation of roGFP2-Orp1. Grayscale and color images were captured for each time point. Ratiometric quantification was performed using ImageJ. Mean pixel intensities were determined from background-subtracted root hair images, and the intensity ratio (UV excitation/blue excitation) was calculated for each treatment from three replicated seedling treatments.

2.9. Statistical analysis

Statistical analyses were performed using the built-in analysis tool in Graphpad Prism (v. 7.00). To determine if NA or AEO exposure lead to a significantly different ($p < 0.05$) organelle or cytoskeletal response, a one-way analysis of variance (ANOVA) was used. A post-hoc Dunnett test was performed for a multiple-to-one comparison of the different NA and AEO treatments to the control data to determine which treatments were significantly different from the control data at the same concentration.

3. Results

We previously reported that Arabidopsis root growth was impaired after treatment with NAs and the AEO fraction (Leishman et al., 2013). Treatment of Arabidopsis seedling roots with a mixture of 10 mg/L single ring NAs (3.33 mg/L of each of three single ring NAs, see Methods and Leishman et al., 2013) revealed that cells near the root tip were swollen and isotropic (rounded) rather than the typical elongated, non-isotropic shape that was observed in untreated roots (Fig. 1). This short root and isotropic cell shape phenotype was similar to that observed in Arabidopsis microtubule mutants or in Arabidopsis roots that were treated with microtubule inhibiting agents (Whittington et al., 2001; Baskin et al., 2004). This observation prompted us to determine whether NA or AEO treatment caused microtubule disruption in plant cells, and whether the structure, organization and dynamics of actin filaments and membrane-bound organelles were also affected by this treatment.

Four types of solution treatment were used to test the cytoskeleton and organelle responses to NA and AEO exposure in epidermal cells. These compounds represented surrogate or model NAs of different classes, as well as the AEO fraction. These treatments were consistent with the those used in our previous study that reported the effects of NAs and AEOs on Arabidopsis growth and development (Leishman et al., 2013). The first was a mixture of three different single ring (SR) surrogate NAs: cyclohexane propionic acid, cyclohexane butyric acid, and cyclohexane pentanoic acid mixed together in equal parts to produce a stock concentration of 100 mg/mL; the second consisted of a surrogate two-ring NA, decahydronaphthalene-2-carboxylic acid (DH); and the third was a model diamondoid NA that was empirically shown to be present in OSPW, 1-adamantanecarboxylic acid (AdCA). In the present study, we treated epidermal layers of scales from onion bulbs and of roots from Arabidopsis seedlings with these compounds. Onion epidermal cells are an excellent model plant cell type due to the efficient transient expression of genes encoding fluorescent protein markers, limited autofluorescence, dynamic subcellular movements, and ease to which the epidermal monolayer can be removed by peeling. Onion bulb epidermal peels are easily treated with compounds of interest by floating peels on solutions that contain the compound. Arabidopsis seedlings can be used to visualize the cytoskeleton and organelles in cells of intact plants, as lines that express a range of fluorescently labelled subcellular structures are readily available.

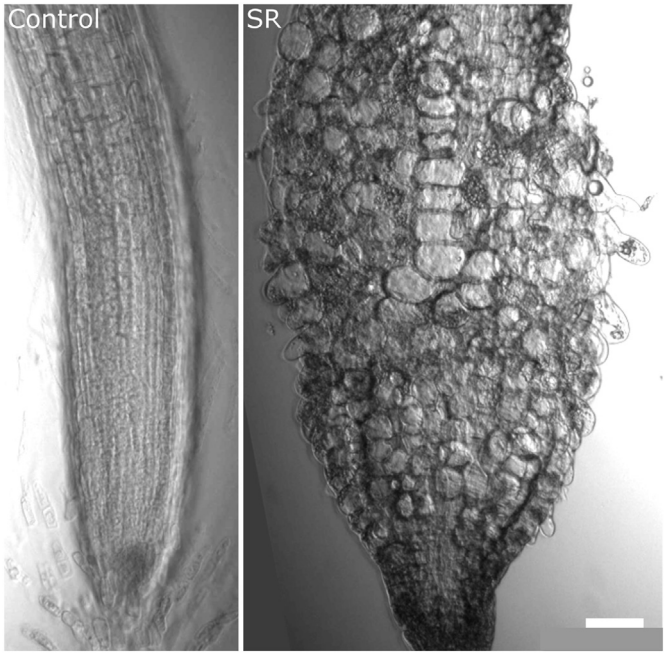

Fig. 1. Arabidopsis root growth after NA exposure. Arabidopsis seedlings were germinated and grown on agar medium without (left panel) or with (right panel) 10 mg/L SR medium (pH 5.0) for 14 days. Bar = 50 μm.

3.1. Effects of NA and AEO treatment on microtubule and actin filament density, organization, and dynamics

The cortical microtubule network of onion epidermal cells was highly sensitive to all NAs and the AEO fraction. A 4 h treatment of cells with 10 mg/L of the single ring NA mixture (SR), 1-adamantane carboxylic acid (AdCA), and the AEO fraction resulted in a significant decrease in cortical microtubule density, while the lowest decahydronaphthalene-2-carboxylic acid (DH) concentration that resulted in a significant decrease was 25 mg/L (Fig. 2A). Exposure to SR was most effective in reducing microtubule integrity, as treatment with 50 mg/L SR eliminated most cortical microtubules from the cell (Fig. 2B). This microtubule disassembly was similar to that observed when onion epidermal cells were exposed to 10 μM of oryzalin (a microtubule destabilizing agent, Fig. 2B). The SR treatment often resulted in fluorescent aggregates of tubulin throughout the cell cortex. Interestingly, exposure to 50 mg/L DH resulted in short, rigid microtubules that often formed clusters attached at a focal point (Fig. 2B). Many of these rigid microtubules oscillated within the cell cortex (Supplemental Movie 1C). A similar microtubule pattern was occasionally observed in cells treated with 50 mg/L AEO for 4 h (Supplemental Movie 1E). Short-term SR treatments (50 mg/L for 15 min) resulted in rapid microtubule disassembly, whereas DH, AdCA and AEO required longer-term treatment times (up to 45 min, Supplemental Fig. 1). Similar to the microtubule responses observed in onion epidermal cells, treatment with NA and AEO (50 mg/L) for 4 h was effective in disrupting microtubules in Arabidopsis root epidermal cells (Fig. 3). AdCA treated cells retained some elongated microtubules, and treatment with the AEO fraction resulted in patches of GFP signal that formed in the cortical region of the cell (Fig. 3).

Actin filament integrity was also affected in cells treated with NAs and the AEO fraction. However, the actin filament effects required higher concentrations of these compounds than for microtubule disassembly, and unusual concentration dependent responses were observed. Onion epidermal cells exposed to SR, DH, and AdCA at concentrations of 10 or 25 mg/L for 4 h resulted in no significant change in actin filament density, while AEO exposure resulted in a decrease in density at 10 mg/L, but showed no difference at 25 or 50 mg/L (Fig. 4A). Treatment with 50 mg/L caused a significant decrease in actin filament density in SR treated cells and an increase in density in AdCA treated cells. Treatment with a higher concentration (75 mg/L) of DH and AEO for 4 h led to significant decreases in actin filament density (Fig. 4A, B). Exposure to latrunculin B (1 μM), a potent actin filament depolymerizer, caused a near complete breakdown of actin filaments (Fig. 4B). Exposure of cells to SR for 4 h at 50 mg/L resulted in actin filaments that were shorter, more branched, and lacked the typical lateral dynamic movements when compared to the actin filaments observed in untreated cells (compare Supplemental Movie 2A with 2B). Treatment with 50 mg/L DH and AEO also affected the lateral movement of actin filaments, although a reduction in actin filament density was not observed for these treated cells (Supplemental Movie 2C and 2E, respectively).

The relative stability of actin filaments in onion epidermal cells after exposure to NAs and AEO suggested that actin filaments were less sensitive to these treatments when compared to cortical microtubules. To verify this observation, co-expression of microtubule and actin filament fluorescent markers was performed in onion epidermal cells. Cortical microtubules in cells exposed to 50 mg/L SR, DH, and AdCA for 1 h showed high levels of disruption, while actin networks within the same cells remained stable (Supplemental Fig. 2). Microtubules were not adversely affected by AEO treatment until the 4 h time point. The organization of actin filaments was only affected by treatment of SR at

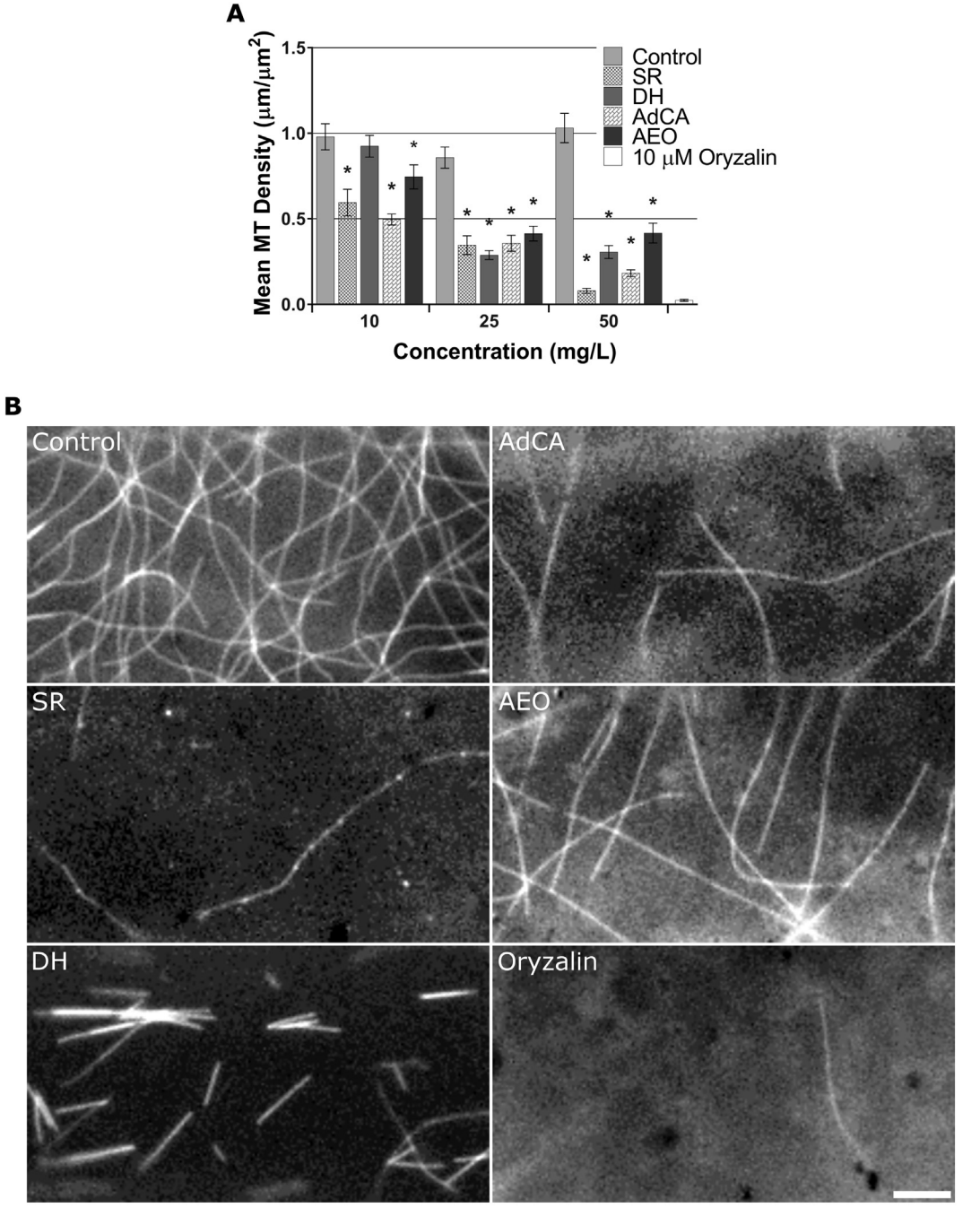

Fig. 2. Responses of onion epidermal cell cortical microtubules to 4 h of NA and AEO treatment. A) Mean microtubule density after treatment with SR, DH, AdCA, the AEO fraction, and 10 μM oryzalin. Mean values ± SEM are based on data from 10 cells. Mean values that are significantly different from the control ($p < 0.05$) within each treatment concentration are indicated (*). B) Representative images of microtubules in onion epidermal cells exposed to 50 mg/L NAs and AEO and 10 μM oryzalin. Bar = 13 μm.

50 mg/L at 2 h, whereas 4 h of DH, AdCA, and AEO exposure did not lead to a considerable disruption of actin filaments (Supplemental Fig. 2).

Actin filaments in root epidermal cells of Arabidopsis seedlings also showed varying levels of disorganization upon NA and AEO treatment. Exposure to NAs and AEO (50 mg/L) for 4 h resulted in visible actin filament breakdown in Arabidopsis root epidermal cells, although not as extensive as in cells treated with latrunculin B (Fig. 5). Roots exposed to SR resulted in a level of actin filament disruption similar to that observed in onion epidermal cells under the same conditions (Fig. 4). While showing signs of disruption, cells exposed to DH also contained numerous circular structures that were interlaced with actin filaments (Fig. 5). The clusters were not dynamic, but appeared to interrupt the actin cytoskeleton by displacing filaments from the cortex. While actin filament density decreased after exposure to AdCA, an actin bundling effect was often visible (Fig. 5).

3.2. Effects of NA and AEO treatment on the dynamics and structure of mitochondria, peroxisomes, and Golgi stacks

Onion epidermal cell exposure to NAs and AEOs resulted in significant changes in the velocity and structure of mitochondria, peroxisomes, and Golgi stacks. The mean maximal velocity of the fastest moving mitochondria, peroxisomes, and Golgi (i.e., the ten highest velocities of each organelle type in an individual cell) was significantly reduced at 25 mg/L in SR and AEO treated cells (Fig. 6A, C, E). The average maximal velocity of organelles in control cells were approximately 2

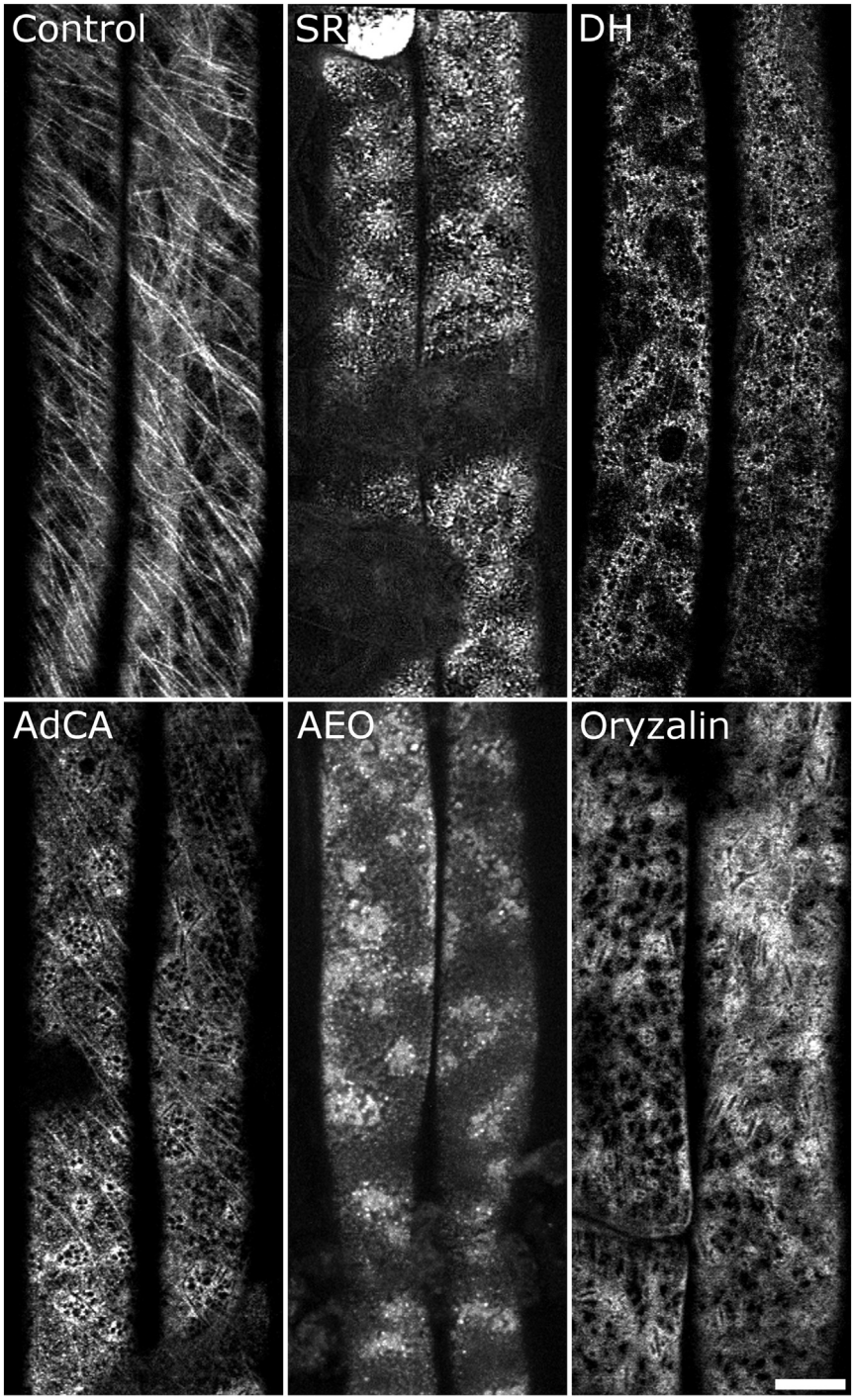

Fig. 3. Arabidopsis root epidermal cell cortical microtubule responses to 4 h NA and AEO treatments. Seedlings stably expressing GFP-MAP4 were treated with 50 mg/L NA and AEO, and 10 μM oryzalin. Bar = 10 μm.

μm/s. Treatment with 50 mg/L of each NA or AEO solution resulted in a significant reduction of organelle velocities in most treatments to approximately 0.2 μm/s (except AdCA, ~1 μm/s). Organelle movements observed in the NA and AEO exposed cells were typically rapid oscillations, compared to frequent single vector movements that were observed in control cells (Supplemental Movies 3, 4 and 5). Interestingly, treatment with 10 mg/L AdCA resulted in elevated velocity of Golgi stacks (Fig. 6E), and velocities of mitochondria also trended upward after treatment with lower concentrations of AdCA (Fig. 6A, C).

Distinct changes in organelle shape and structure were observed in onion epidermal cells treated with NAs and AEO fraction. Peroxisomes and mitochondria showed a mixture of spherical and elongated shapes, extending several microns in length (top panels in Fig. 6B, D). In contrast, all treatments at 50 mg/L for 4 h caused mitochondria and peroxisomes to become spherical (Fig. 6B, D). Additionally, many of the peroxisomes in treated cells became enlarged, particularly in cells exposed to SR (Fig. 6D). The spherical response of mitochondria and peroxisomes was observed as early as 15 min after the initial NA and AEO exposure, and coincided with the early signs of microtubule disruption (Supplemental Fig. 3). Golgi stack morphology was also affected in treated onion epidermal cells. Under control conditions, Golgi stacks displayed a characteristic crescent shape due to the cis-trans polarity

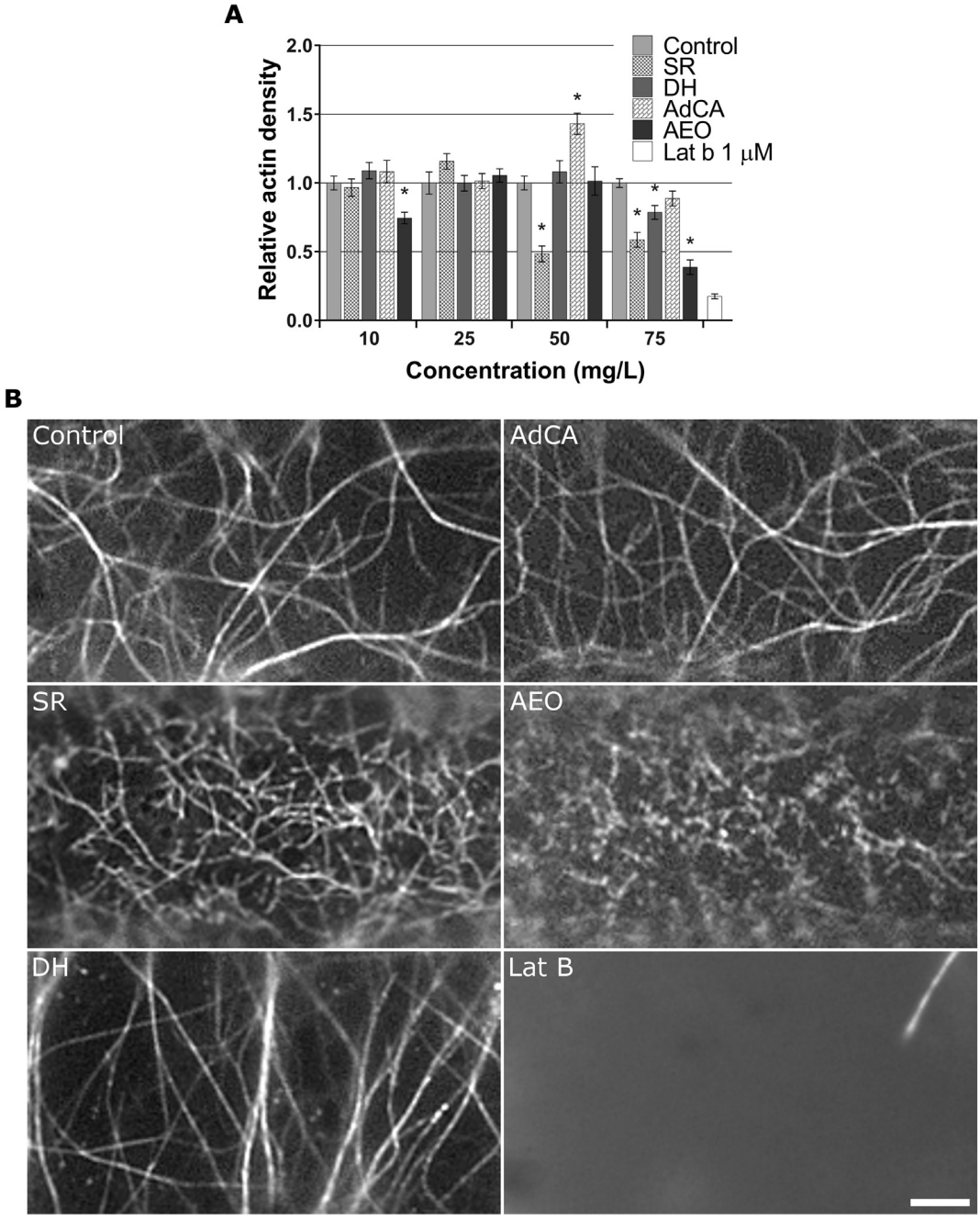

Fig. 4. Responses of onion epidermal cell actin filaments to 4 h NA and AEO treatments. A) Relative density measurements of cortical actin filament networks in onion epidermal cells after 4 h of treatment with SR, DH, AdCA, the AEO fraction and 1 μM latrunculin B (Lat B). Values are normalized to control roots. Mean values ± SEM are based on a data from 10 cells. Mean values that are significantly different from the control ($p < 0.05$) within each treatment concentration are indicated (*). B) Representative images of actin filaments in onion epidermal cells exposed to 75 mg/L NAs and AEO and 1 μM latrunculin B. Bar = 8 μm.

of the organelle (Fig. 6F inset). Normal sized and smaller, fragmented Golgi structures that were still capable of movement were observed after treatment with 25 mg/L of NA and AEO (data not shown). Exposure to 50 mg/L of SR, DH, and AEO exacerbated Golgi stack fragmentation, whereas 50 mg/L treatment with AdCA had a lesser effect on the structure of Golgi stacks than the other treatments (Fig. 6F). Changes in Golgi stack morphology were observed as early as 15 min after SR exposure, whereas there was no morphological response after the same time period when exposed to DH, AdCA, and AEO (Supplemental Fig. 3). When onion epidermal cells were treated with oryzalin, the loss of microtubules did not have appreciable impact of the morphology and movements of mitochondria, peroxisomes and Golgi (data not shown). Latrunculin B treatment resulted in the cessation of mitochondria, peroxisomes and Golgi movement, and the organelles became tightly clustered within the cell (data not shown). These general observations of organelle morphology and dynamics have been made previously in other plant cell studies that used cytoskeleton destabilizing agents (e.g., Chuong et al., 2005; Nebenführ et al., 1999; Van Gestel et al., 2002; Satiat-Jeunemaitre et al., 1996).

Mitochondria, peroxisomes and Golgi stacks were observed in Arabidopsis root epidermal cells to determine whether the organelle velocity and shape effects of NA and AEO treatment were consistent with that observed in onion epidermal cells. These organelles showed dynamic movements in untreated Arabidopsis root epidermal cells, with a portion of organelles moving at high velocities at any point in time (Supplemental Movies 6 to 8). Mitochondria and peroxisomes in

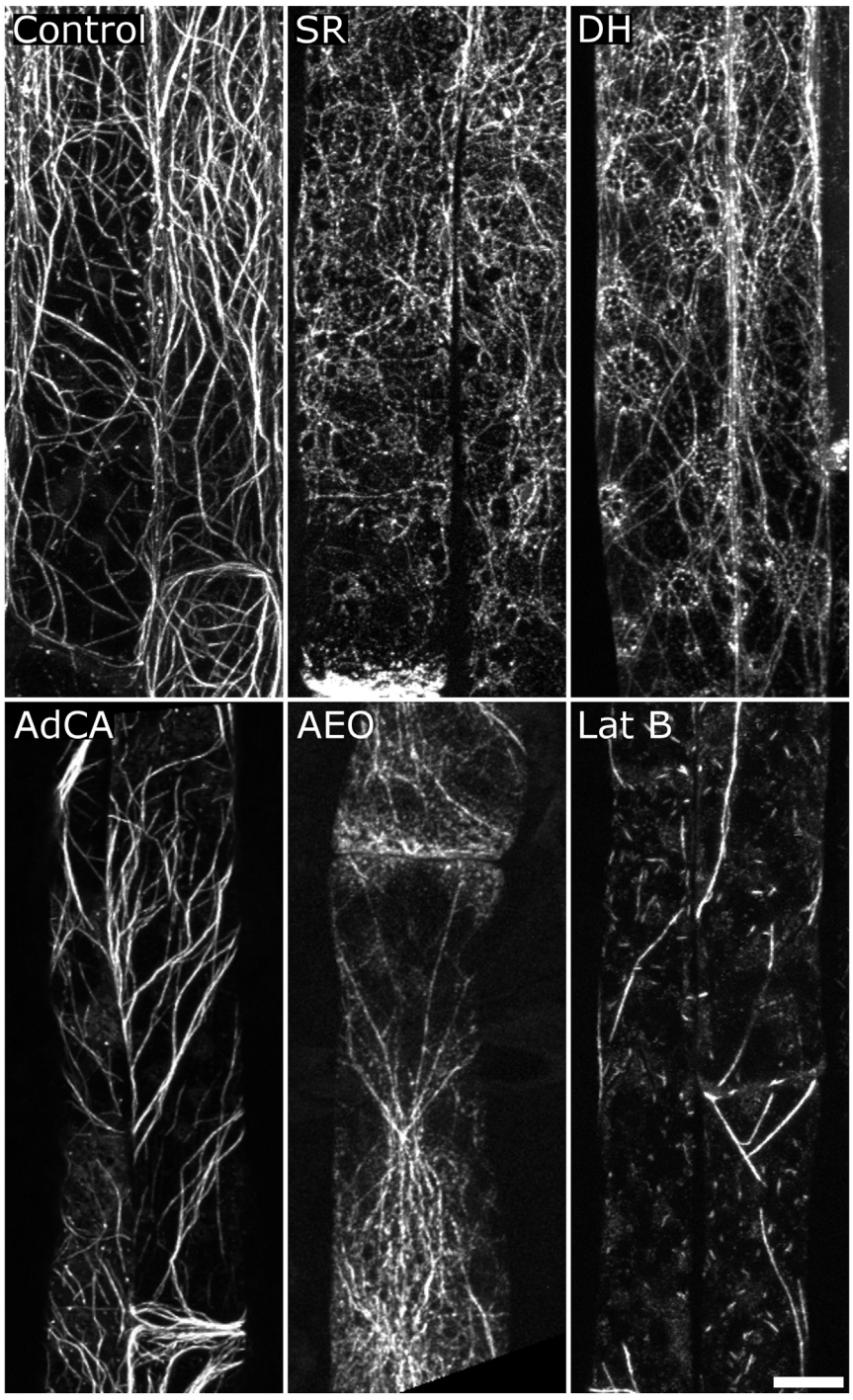

Fig. 5. Arabidopsis root epidermal cell cortical actin filament responses to 4 h NA and AEO fraction treatments. Seedlings were treated with 50 mg/L NA and AEO solutions, and 1 μM latrunculin B. Bar = 10 μm.

untreated cells were typically a mixture of spherical and elongated shaped structures (Supplemental Figs. 4, 5). Golgi stacks in untreated cells appeared punctate with fluorescence uniformly distributed throughout the organelle (Supplemental Fig. 6), unlike the crescent shape Golgi fluorescence observed in untreated onion epidermal cells (Fig. 6F). Exposure to 50 mg/L NAs and AEO for 4 h resulted in nearly complete cessation of organelle movement (Supplemental Figs. 4, 5, and 6; Supplemental Movies 6, 7 and 8). Unlike onion epidermal cell organelles that were capable of some movement after AdCA treatment (~1 μm/s) (Fig. 6A, C, E), Arabidopsis root epidermal cell mitochondria, peroxisomes and Golgi did not exhibit movement after similar treatments to the NAs and AEO.

In Arabidopsis root epidermal cells, treated mitochondria took on a spherical morphology that was similar to what was observed in onion cells (Supplemental Fig. 4). Arabidopsis peroxisomes were spherical in shape after exposure to 50 mg/L SR, AdCA, and AEO for 4 h. However, DH treatment caused peroxisomes to take on an irregular shape that were connected by visible narrow extensions (Supplemental Fig. 5), often referred to peroxules in previous studies (Jaipargas et al., 2016). The irregularly shaped peroxisomal phenotype was not seen in onion epidermal cell peroxisomes, indicating a possible difference in how the two plant cell types respond to DH exposure. Golgi stacks showed unusual irregular and elongated shapes, particularly in the DH and AdCA treated cells (Supplemental Fig. 6).

3.3. Effects of NA and AEO treatment on the organization and dynamics of the endoplasmic reticulum

The morphology and dynamics of the ER were also affected by NA and AEO treatment in onion and Arabidopsis epidermal cells. In control onion epidermal cells, the ER network is reticulate throughout the cell cortex, with thin tubules connecting flat cisternae (Fig. 7B). These tubules displayed dynamic movements, resulting in new connections with other tubules and cisternae (Supplemental Movie 9). Cell exposure to 25 mg/L of each type of NA, but not the AEO fraction, resulted in a significant decrease in total ER tubule length (Fig. 7A). Exposure to 50 mg/L of SR resulted in the most noticeable change in ER structure, with the

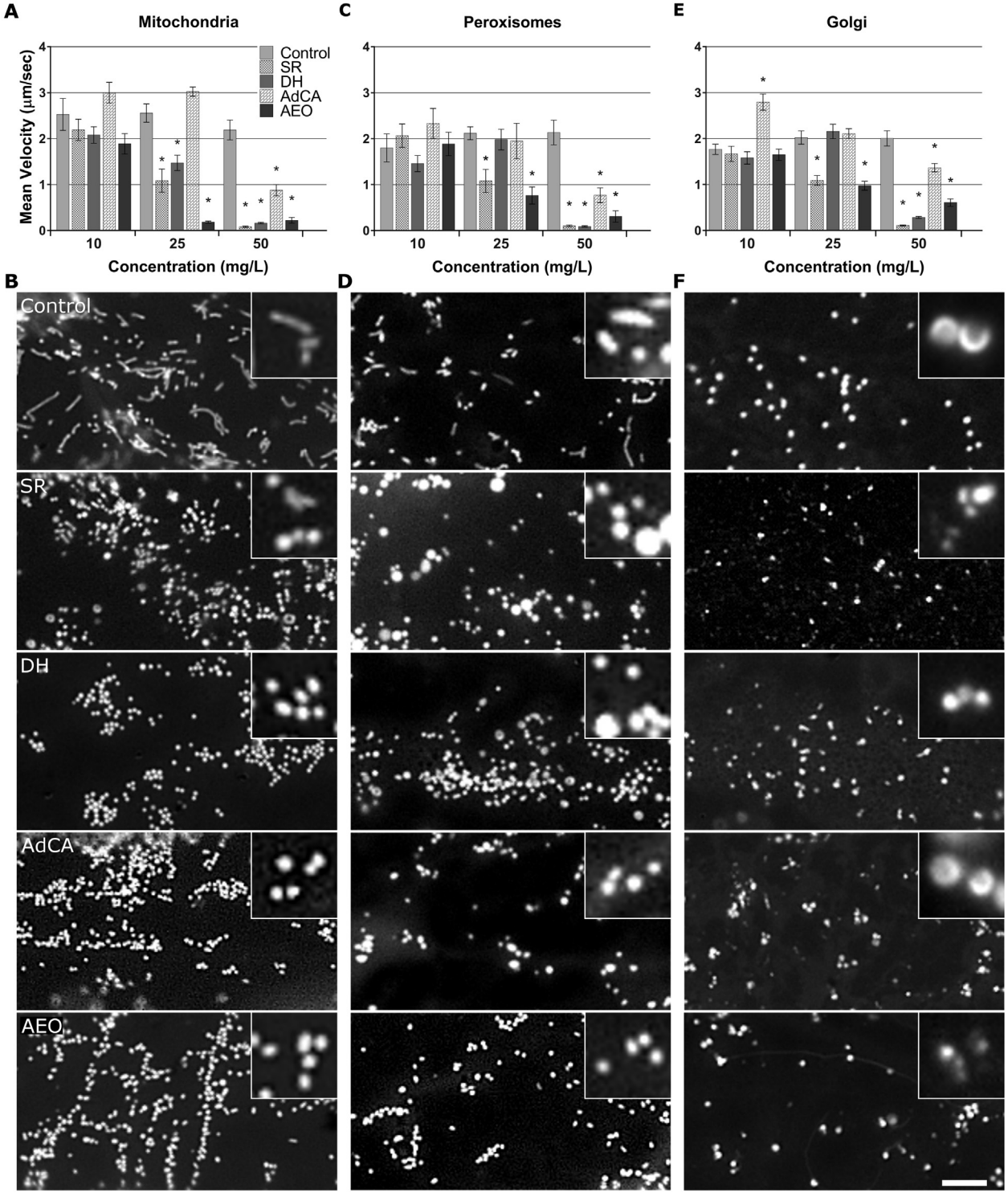

Fig. 6. Responses of onion epidermal cell mitochondria, peroxisomes, and Golgi stacks to a 4 h NA and AEO treatment. (A, C, E) Mean maximal velocities of mitochondria, peroxisomes, and Golgi stacks after treatment with NAs and the AEO fraction at concentrations of 10, 25, and 50 mg/L. Mean values ± SEM are based on a value of $n = 10$ cells for mitochondria and peroxisomes, and $n = 5$ cells for Golgi stacks. Mean values that are significantly different from the control ($p < 0.05$) within each treatment concentration are indicated (*). (B, D, F) Representative images of mitochondria, peroxisomes, and Golgi arrangement and structure after NA and AEO treatment at 50 mg/L. Insets are representative organelles of each treatment magnified 20 fold. Bar = 8 µm.

development of punctate fluorescent foci, shorter tubules, and cisternae that did not show the same level of dynamics as control cells (Fig. 7B; Supplemental Movie 9B). Disruption of the ER was not as obvious in the DH, AdCA and AEO treated cells, and there was visible ER dynamic movements that were greater than in SR exposed cells (Fig. 7B, Supplemental Movie 9). Disruption of the cytoskeleton in onion epidermal cells by treatment with oryzalin and/or latrunculin B (singly or together) caused some changes in ER morphology that included reduced ER density and larger, irregularly shaped cisternae (Supplemental Fig. 7). However, these changes in ER morphology did not resemble ER morphologies in the NA and AEO treated onion epidermal cells (Fig. 7).

The ER in Arabidopsis root epidermal cells was also sensitive to NA and AEO treatments. The cortical ER in control cells had a reticulate structure with cisternae connected by thin tubules (Fig. 8). The GFP marker expressed in this line also labelled highly fluorescent fusiform bodies that contain vegetative storage proteins, as typically observed in seedling epidermal cells (Fig. 8) (Nelson et al., 2007). Exposure to 50 mg/L SR for 1 h resulted in a breakdown of much of the reticulate structure, and the fusiform bodies took on a spherical appearance. Disruption to the ER was further enhanced after 4 h of SR exposure. Cells exposed to DH and AdCA for 1 h maintained their reticulate ER structure, but showed enhanced cisternal surface areas (Fig. 8). After 4 h, SR, DH and AEO cells showed a range of disrupted ER patterns, and the fusiform bodies tended to be spherical (Fig. 8). The integral disruption of the ER tubules in AEO treated cells was extensive, compared to the other treatments. The severity of ER membrane disruption in these cells indicates that the ER may be more sensitive to AEO exposure than individual NA exposure in Arabidopsis root epidermal cells.

3.4. Cell viability, organelle recovery and ROS production in NA and AEO treated cells

Cell viability staining was used to determine whether reduced viability of onion epidermal cells occurs after NA and AEO treatment. Exposure of cells to 50 mg/L of the NA solutions for 4 h followed by propidium iodide staining did not show nuclear staining, indicating that NA exposure did not alter cell viability (Fig. 9). In contrast, cells exposed to 50 mg/L of the AEO solution for 4 h resulted in nuclear staining in approximately 40% of cells (Fig. 9). In support of this observation, transient expression of fluorescent protein organelle and cytoskeleton markers in AEO treated cells, followed by propidium iodide staining, revealed that only viable cells were able to express the fluorescent markers (data not shown). These data suggest that extended treatment of epidermal cells with the AEO fraction, but not the NAs, results in reduced cell viability.

These cell viability results prompted us to determine whether the cytoskeleton and organelles in NA and AEO treated onion epidermal cells could return to their pre-treatment state after these compounds were washed away from the cells. A 4 h treatment with NA and AEO (50 mg/L) was used to disrupt the microtubule network, followed by rinsing the cells for 1 h with solutions lacking these compounds. The organization of the microtubule network in washed NA treated cells recovered and was comparable in appearance to microtubules in control cells (Supplemental Fig. 8). In contrast, the microtubule network in AEO treated cells did not recover after washing. Similarly, the velocity of Golgi stacks in washed AEO treated cells did not return to normal after washing, and the disrupted Golgi stack morphology in these washed AEO cells also did not recover (Supplemental Fig. 9). These findings are consistent with the cell viability studies described above that demonstrate that AEO treatment resulted in reduced cell viability compared to NA treatments.

A common cellular response to environmental stress is the production of reactive oxygen species (ROS). We tested whether Arabidopsis root hairs accumulate significant levels of ROS in response to AEO exposure. Root hairs are an extension of an epidermal cell and function to increase the surface area of the root for water and nutrient absorption, and assist in anchoring the plant within the soil. They are dynamic cells that demonstrate rapid cytoplasmic streaming, and provide a slender cell type that can be directly exposed to toxic compounds and imaged with limited manipulation. The Arabidopsis roGFP2-Orp1 line is an ideal tool to sense cytosolic H_2O_2 production in root hairs in a pH-insensitive manner (Scuffi et al., 2018). Cytosolic H_2O_2 results in a decrease in roGFP2 fluorescence when excited with blue light. Excitation of the same cell with UV-light provides a self-normalizing, ratiometric readout for H_2O_2 abundance. Roots from 10-day old Arabidopsis roGFP2-Orp1 seedlings that were exposed to 100 mg/L AEO or 10 mM H_2O_2 for 10 min showed a decrease in the fluorescence intensity of blue light-excited GFP fluorescence relative to control root hairs (Fig. 10A). Treated root hairs continued to demonstrate normal cytoplasmic streaming, indicating that they remained alive during the treatment periods. Ratiometric analysis demonstrated that there was a significant difference in the abundance of H_2O_2 in root hairs treated with the AEO fraction compared to control root hairs (Fig. 10B). The AEO-induced fluorescence response was similar to H_2O_2 treatment (Fig. 10A, B). These results indicate that exposure to AEO fraction leads to oxidation of roGFP2-Orp1 through the accumulation of H_2O_2 in the cytosol of root hairs.

4. Discussion

The dynamics, organization and integrity of intracellular structures in plant cells can change dramatically in response to biotic and abiotic stress signals (Mathur et al., 2012). Real time, high-resolution fluorescence imaging of organelles and the cytoskeleton has provided valuable insight into these cellular responses. For instance, aluminum stress caused rapid changes in microtubule bundling and microtubule orientation in root cells (Schwarzerová et al., 2002), and peroxisomes in hypocotyl cells exhibited dynamic shape changes and higher division rates in response to intense light and exposure to ROS (Jaipargas et al., 2016). Here, we report extensive disruption to the structure, organization, and dynamics of the cytoskeleton and membrane-bound organelles in the epidermal cells of onion scales and Arabidopsis roots in response to short-term exposure with NAs and the AEO fraction of OSPW. Arabidopsis and onion are divergent plant species that represent the two major angiosperm lineages, suggesting that these cellular responses are common across the plant kingdom. Many of these responses were observed within the initial 15 min of exposure (Supplemental Figs. 1 and 3). Interestingly, treatment with the AEO fraction resulted in the highest level of toxicity, as revealed by reduced viability of onion epidermal cells (Fig. 9) and by the lack of recovery of microtubule and Golgi structure and dynamics in surviving cells after AEO washout from cells (Supplemental Figs. 8 and 9). The AEO fraction contains a complex mixture of organic compounds that includes classically defined NAs as well as SO^-, SO_2^-, and NO_2^- containing molecules, and specific sub-fractions of AEO are known to possess higher toxicity than others (Frank et al., 2008; Morandi et al., 2015). Thus, the enhanced cellular toxicity of the AEO fraction, compared to the single classes of NAs used in this study, may result from the additive effects of numerous highly toxic compounds within the AEO fraction.

The widespread cellular effects that were observed in NA and AEO treated cells suggest that a general stress response is elicited at the cellular level. Exposure of onion epidermal cells to the three types of NAs used here resulted in cellular responses that were reversible, indicating that programmed cell death response was not induced. Additionally, in NA and AEO treated cells there was an absence of cellular phenotypes that were previously shown to be associated with apoptotic plant cell death (e.g., plasma membrane blebbing and nuclear deformation, Dickman et al., 2017). The rapid production of ROS in treated Arabidopsis root hairs (Fig. 10) indicates that oxidative stress may contribute to these cellular responses. This observed increase in ROS is consistent with our previous gene expression data that showed the

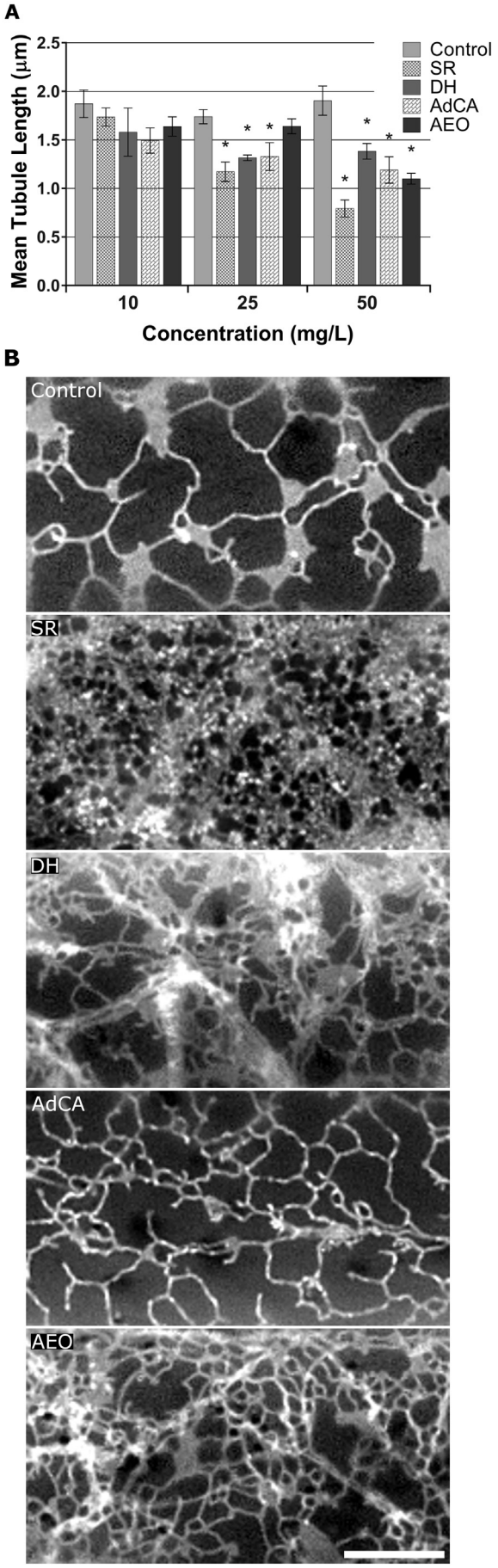

induction of numerous genes involved in oxidative stress in Arabidopsis roots exposed to AEO (Widdup et al., 2015). Increased levels of ROS and activation of genes related to oxidative stress have also been observed in studies related to OSPW effects on animal and bacterial cells and may contribute to the mechanism of OSPW toxicity in these species (Morandi et al., 2017; Wiseman et al., 2013; He et al., 2012). A study using a human cell line demonstrated that polyoxygenated compounds, rather than classical NAs, were the primary component of the AEO fraction that triggered oxidative stress (Sun et al., 2017).

ROS production is a common feature of environmental stress signaling that regulates numerous cellular processes (Waszczak et al., 2018). Altered ROS levels can trigger visible changes to cell structure and organization, some of which are consistent with our observations in NA and AEO treated cells. For instance, ROS production induced by abiotic stress in plants can cause microtubule reorganization or disassembly that elicits downstream signals leading to adaptive events in the cell (Livanos et al., 2014; Nick, 2013). In Arabidopsis, treatment of leaves with ROS and ROS-inducing chemicals caused elongated mitochondria to take on a spherical shape (Yoshinaga et al., 2005), as did exposure to cadmium (Lee and Back, 2017). The effect of ROS on organelle shape can differ depending on the stress situation. ROS treatment and exposure to high light intensity (a ROS stimulating stress) triggered an increase in peroxule abundance in Arabidopsis hypocotyl cells, followed by peroxisome elongation and fission (Sinclair et al., 2009). This outcome was thought to provide an increase in peroxisome number to assist in overcoming cellular stress. In contrast, our observations showed that NA and AEO caused peroxisomes to stall and take on a spherical appearance (and occasional peroxisome swelling) in Arabidopsis roots and onion epidermal cells (Fig. 6D and Supplemental Fig. 5). These observations of peroxisome stalling and spherical size increase were similar to that in Arabidopsis hypocotyl cells exposed to hypoxic stress (Sinclair et al., 2009).

The observed changes in organelle morphology in treated cells may be directly due to the structural characteristics of NAs. Many NAs are amphipathic molecules (i.e., hydrophilic carboxylic acid and hydrophobic alkyl group) which led to the hypothesis that their integration into cellular membranes causes membrane disruption (narcosis) (Frank et al., 2008; Zhang et al., 2016). Accordingly, NAs would first integrate into the plasma membrane and then partition into organelle membranes. This integration could cause abnormal organelle morphology and reduced organelle function, as well as detrimental changes to the structure and function of the plasma membrane. Our observation that chemical disruption of microtubules and actin filaments did not result in changes in the morphology or mitochondria, peroxisomes and Golgi stacks indicates that cytoskeletal disruption does not signal general NA and AEO-induced changes in organelle shape. This lack of cytoskeleton effect on organelle shape lends support to the narcosis hypothesis, where integration of NAs into organelle membranes could result in visible organelle shape changes. The severity of membrane damage by a xenobiotic compound has been correlated with its lipophilicity and size (Protić and Sabljić, 1989; Schultz, 1989). The molecular weights of NAs used in this study are relatively low (molecular weight range of 156 to 184) compared to range of molecules present in the total organic fraction. Thus, the greater complexity of the AEO fraction may result in increased disruption of membrane function and could explain why the AEO fraction showed greater cellular toxicity (Fig. 9).

We observed that the NA and AEO treatments also resulted in a general decrease in organelle movement. Myosin driven organelle movement along actin filaments in plant cells is thought to generate cytoplasmic streaming that aids in positioning of organelles and macromolecules (Geitmann and Nebenführ, 2015). Actin filaments were relatively intact at 50 mg/L NA and AEO treatment, except in the SR treated

Fig. 7. Responses of onion epidermal cell ER to a 4 h NA and AEO treatment. A) Mean tubule length in cells exposed to 10, 25, and 50 mg/L of each treatment. B) Representative images of cortical ER after NA and AEO treatment (50 mg/L). Mean values ±SEM are based on n = 5 cells. Mean values that are significantly different from the control ($p < 0.05$) within each treatment concentration are indicated (*). Bar = 8 μm.

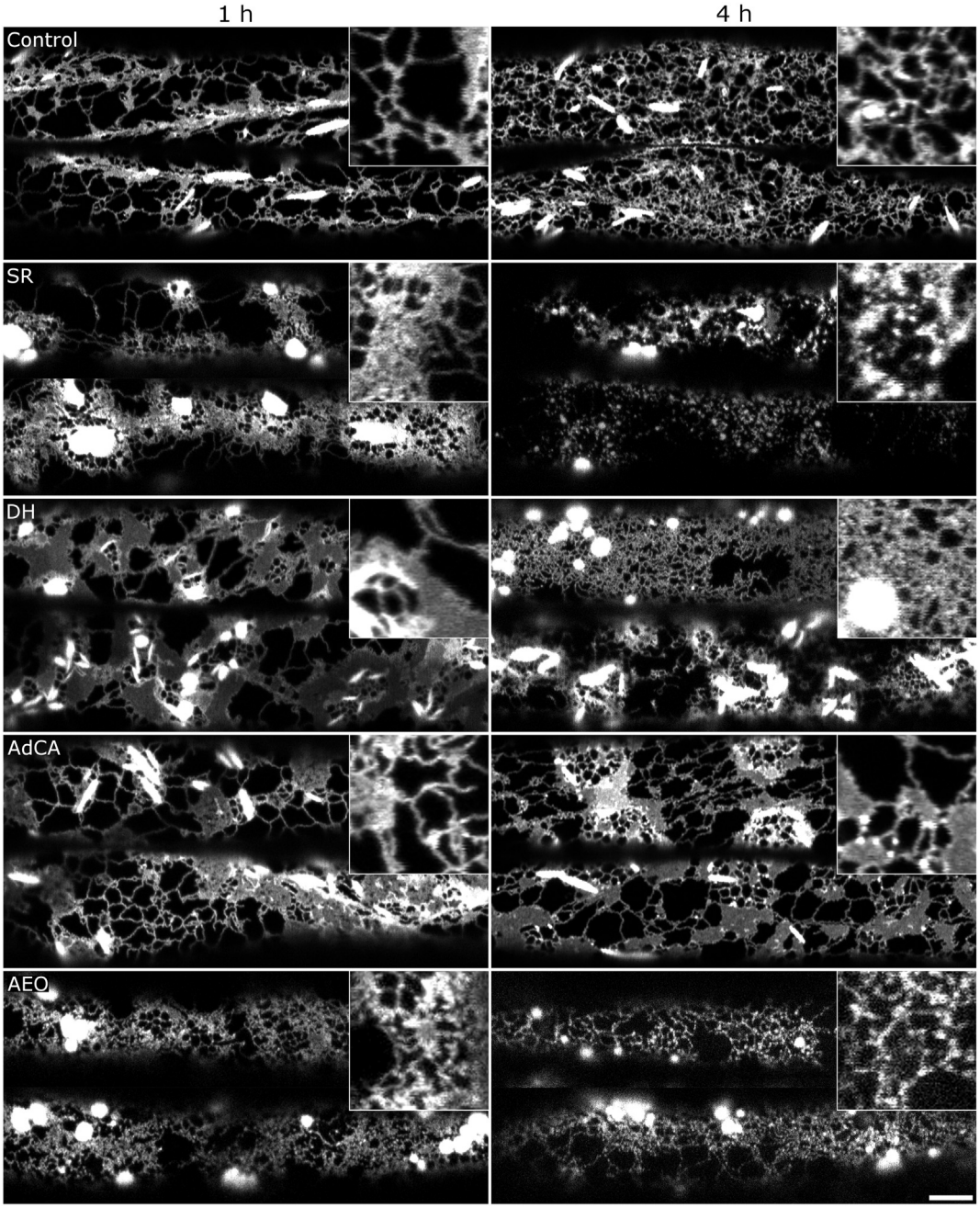

Fig. 8. Arabidopsis root epidermal cell ER after NA and AEO treatment. Cells were treated with 50 mg/L NA and AEO for 1 and 4 h (50 mg/L). Insets are representative organelles of each treatment magnified 2 fold. Bar = 10 μm.

cells (Fig. 4A). However, the mitochondrial, peroxisomal and Golgi movement was effectively eliminated in cells treated with NAs and the AEO fraction and greatly reduced in the AdCA treated cells (Fig. 6A, Supplemental Movies 3–8). While these organelle movements typically ceased in onion epidermal cells upon NA and AEO treatment (50 mg/L), the ER continued to demonstrate dynamic movements (Supplemental Movie 9). These observations suggest that changes in organelle membrane dynamics and/or shape may affect inter-organelle interactions. One of the models for organelle movement in plant cells proposes that ER movement is driven directly by the actin-myosin machinery, and the movement of other organelles is indirect via tethering to the ER (Nebenführ and Dixit, 2018; McKenna et al., 2018). In cells treated with NAs and the AEO fraction, this organelle tethering to the ER might be disrupted, while still retaining the ER association with stable actin filaments via myosin motors. In this scenario, the ER would continue to demonstrate dynamic movements whereas other membrane-bound organelles would remain static.

Changes to cell structure and function after stress treatment can result in morphological changes at the whole plant level. Indeed, the shortened root phenotype of Arabidopsis seedlings in response to NA and AEO treatment (Fig. 1; Leishman et al., 2013) may be due, in part, to changes in the organization of microtubules. Rather than having a NA/AEO signaling role, microtubule disruption may be central in causing aberrant root growth in response to this stress. The integrity of microtubules is essential for normal cell elongation during root growth because the orientation of cortical microtubules determines the pattern of cellulose microfibril deposition, and this contributes to anisotropic cell growth in elongating roots (Paredez et al., 2006; Crowell et al., 2011). Microtubule-associated proteins (MAPs) that influence microtubule organization can be regulated directly by ROS or through mitogen-

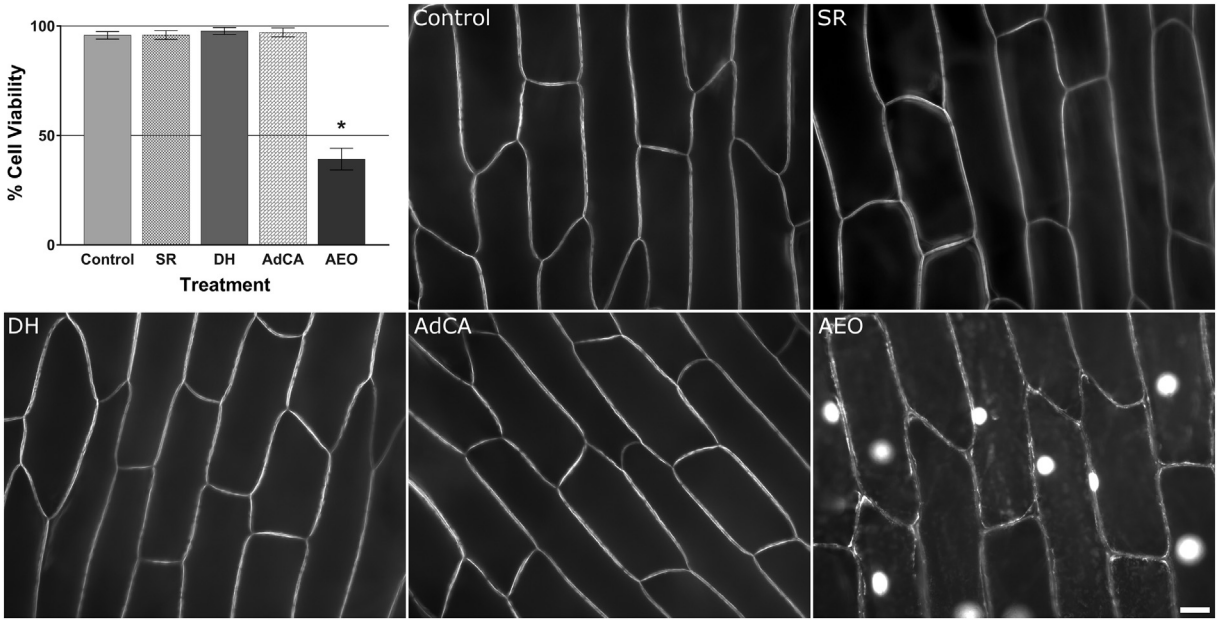

Fig. 9. Viability assay of onion epidermal cells after treatment with NAs and AEO. Cells were treated with 50 mg/L NA and AEO for 4 h. Cells were stained with propidium iodide for 30 min and the percentage of nuclear stained cells was determined (top left panel). Mean values ± SEM are based on data from 100 cells. Mean values that are significantly different from the control ($p < 0.05$) within each treatment concentration are indicated (*). Also shown are representative images of onion epidermal cells after NA or AEO exposure and propidium iodide staining. Bar = 20 μm.

associated protein kinase (MAPK) pathways activated by ROS (Livanos et al., 2014). Elevated levels of ROS elicited by NA/AEO stress could target MAPs and lead to microtubule disruption and abnormal cellulose deposition. Cellulose deposition could also be affected by Golgi dysfunction. Plant Golgi stacks are dynamic organelles that are involved in cellulose synthase complex trafficking to the plasma membrane (McFarlane et al., 2014). The structural disruption of this organelle by NAs and AEOs could result in improper delivery of cellulose synthase complexes to the membrane and ultimately affect the pattern of nascent cellulose synthesis.

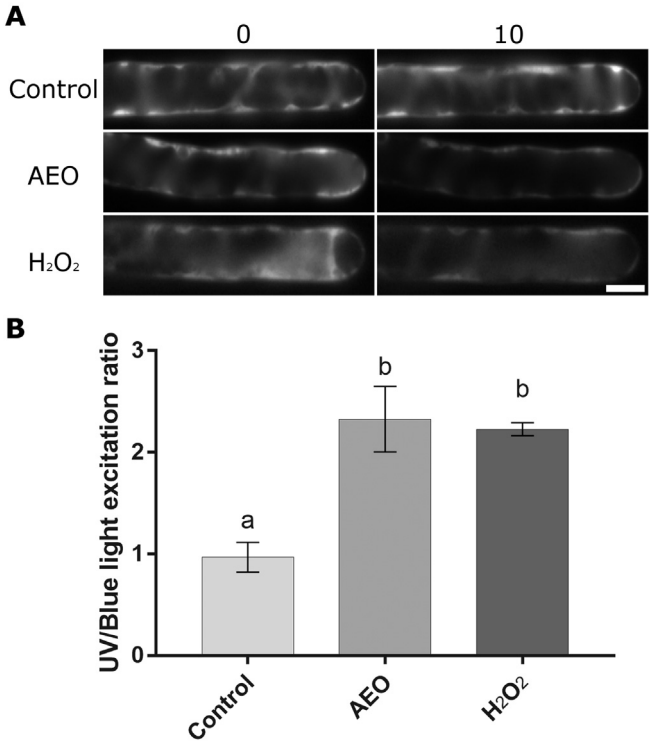

Fig. 10. Response of Arabidopsis roGFP2-Orp1 root hairs to AEO and H_2O_2 treatments. A) Representative images of root hairs expressing roGFP2-Orp1 in Arabidopsis seedlings imaged under blue excitation light at time 0 min and 10 min for each treatment; DMSO control, 100 mg/L AEO and 10 mM H_2O_2. Bar = 10 μm. B) Ratiometric measurement of the root hair response after 10 min exposure to the treatment solutions. Values are based on the ratio of mean fluorescence intensity of UV and blue light excitation of the roGFP probe. Mean values ± SEM are based on a data from three root hairs. Significant differences ($p < 0.05$) between treatments are indicated by different letters.

The mechanisms responsible for the disruption of organelles and cytoskeleton of plant cells after NA and AEO exposure appear complex. The cellular responses might be transient, allowing the cells to survive for a short period until other survival strategies take over. For instance, we observed that Arabidopsis seedling primary roots are arrested in their growth by exposure to NAs and AEO, and newly formed adventitious roots develop at the root-shoot junction (S. Olsen & D.G. Muench, unpublished results). These adventitious roots could allow the plant to access less toxic water at the surface of the soil where rainfall accumulates. This type of developmental response, as well as longer-term tissue level detoxification mechanisms, could facilitate plant tolerance to AEOs. Endophytic microbes could also provide means to facilitate NA degradation and enhance plant survival, as has been observed with plant exposure to other environmental contaminants (Doty et al., 2017). The findings reported here provide the first steps in the characterization of subcellular responses of cells to NA and AEO exposure. These results identify possible areas of research that may further elucidate the complex interactions between plant cells and NAs that may ultimately have a role in signaling and development, as well as identify modes of detoxification. The development of NA-sensitive cellular markers could also provide a simple in vivo tool that serves to sense the most toxic compounds present in the AEO fraction of OSPW, and could also be used to monitor the efficiency of NA degradation in OSPW remediation strategies.

Supplementary data to this article can be found online at https://doi.org/10.1016/j.scitotenv.2018.10.181.

Acknowledgements

Plasmids and Arabidopsis marker lines were generously provided by Andreas Meyer, Richard Cyr, Elison Blancaflor, Andreas Nebenführ and

Takashi Hashimoto. We are grateful to Marcus Samuel for use of his confocal microscope. Financial support for this research was provided by Canada's Oil Sands Innovation Alliance (COSIA) and the University of Calgary.

References

Allen, E.W., 2008. Process water treatment in Canada's oil sands industry: I. Target pollutants and treatment objectives. J. Environ. Eng. Sci. 7 (2), 123–138. https://doi.org/10.1139/S07-038.

Apostol, K.G., Zwiazek, J.J., MacKinnon, M.D., 2004. Naphthenic acids affect plant water conductance but do not alter shoot Na+ and Cl− concentrations in jack pine (*Pinus banksiana*) seedlings. Plant Soil 263 (1–2), 183–190. https://doi.org/10.1023/B:PLSO.0000047725.04930.bc.

Armstrong, S.A., Headley, J.V., Peru, K.M., Germida, J.J., 2009. Differences in phytotoxicity and dissipation between ionized and nonionized oil sands naphthenic acids in wetland plants. Environ. Toxicol. Chem. 28 (10), 2167–2174. https://doi.org/10.1897/09-059.1.

Baskin, T. I., Beemster, G. T. S., Judy-March, J. E., & Marga, F. (2004). Disorganization of cortical microtubules stimulates tangential expansion and reduces the uniformity of cellulose microfibril alignment among cells in the root of Arabidopsis. Plant Physiol., 135 (4), 2279–90. dooi:https://doi.org/10.1104/pp.104.040493.

Bauer, A.E., Frank, R.A., Headley, J.V., Peru, K.M., Hewitt, L.M., Dixon, D.G., 2015. Enhanced characterization of oil sands acid-extractable organics fractions using electrospray ionization-high-resolution mass spectrometry and synchronous fluorescence spectroscopy. Environ. Toxicol. Chem. 34 (5), 1001–1008. https://doi.org/10.1002/etc.2896.

CAPP, 2015. The Facts on: Oil Sands. Canadian Association of Petroleum Producers (CAPP), pp. 1–35. http://doi.org/2015-0014.

Chuong, S.D.X., Park, N.-I., Freeman, M.C., Mullen, R.T., Muench, D.G., 2005. The peroxisomal multifunctional protein interacts with cortical microtubules in plant cells. BMC Cell Biol. 6, 40. https://doi.org/10.1186/1471-2121-6-40.

Clemente, J.S., Fedorak, P.M., 2005. A review of the occurrence, analyses, toxicity, and biodegradation of naphthenic acids. Chemosphere 60, 585–600. https://doi.org/10.1016/j.chemosphere.2005.02.065.

Crowe, A.U., Han, B., Kermode, A.R., Bendell-Young, L.I., Plant, A.L., 2001. Effects of oil sands effluent on cattail and clover: photosynthesis and the level of stress proteins. Environ. Pollut. 113, 311–322.

Crowell, E.F., Timpano, H., Desprez, T., Franssen-verheijen, T., Emons, A., Hofte, H., Vernhettes, S., 2011. Differential regulation of cellulose orientation at the inner and outer face of epidermal cells in the *Arabidopsis* hypocotyl. Plant Cell 23, 2592–2605. https://doi.org/10.1105/tpc.111.087338.

Dickman, M., Williams, B., Li, Y., De Figueiredo, P., Wolpert, T., 2017. Reassessing apoptosis in plants. Nat. Plants 3, 773–779. https://doi.org/10.1038/s41477-017-0020-x.

Doty, S.L., Freeman, J.L., Cohu, C.M., Burken, J.G., Firrincieli, A., Simon, A., ... Blaylock, M.J., 2017. Enhanced degradation of TCE on a superfund site using endophyte-assisted poplar tree phytoremediation. Environ. Sci. Technol. 51, 10050–10058. https://doi.org/10.1021/acs.est.7b01504.

Frank, R.A., Kavanagh, R., Burnison, B.K., Arsenault, G., Headley, J.V., Peru, K.M., ... Solomon, K.R., 2008. Toxicity assessment of collected fractions from an extracted naphthenic acid mixture. Chemosphere 72, 1309–1314. https://doi.org/10.1016/j.chemosphere.2008.04.078.

Fu, L., Li, C., Lillico, D.M.E., Phillips, N.A.I., Gamal El-Din, M., Belosevic, M., Stafford, J.L., 2017. Comparison of the acute Immunotoxicity of nonfractionated and fractionated oil sands process-affected water using mammalian macrophages. Environ. Sci. Technol. 51 (15), 8624–8634. https://doi.org/10.1021/acs.est.7b02120.

Geitmann, A., Nebenführ, A., 2015. Navigating the plant cell: intracellular transport logistics in the green kingdom. Mol. Biol. Cell 26 (19), 3373–3378. https://doi.org/10.1091/mbc.E14-10-1482.

Giesy, J.P., Anderson, J.C., Wiseman, S.B., 2010. Alberta oil sands development. PNAS 107 (3), 951–952. https://doi.org/10.1073/pnas.0912880107.

Grewer, D.M., Young, R.F., Whittal, R.M., Fedorak, P.M., 2010. Naphthenic acids and other acid-extractables in water samples from Alberta: what is being measured? Sci. Total Environ. 408 (23), 5997–6010. https://doi.org/10.1016/j.scitotenv.2010.08.013.

He, Y., Patterson, S., Wang, N., Hecker, M., Martin, J.W., El-Din, M.G., ... Wiseman, S.B., 2012. Toxicity of untreated and ozone-treated oil sands process-affected water (OSPW) to early life stages of the fathead minnow (Pimephales promelas). Water Res. 46 (19), 6359–6368. https://doi.org/10.1016/j.watres.2012.09.004.

Higaki, T., Kutsuna, N., Sano, T., Kondo, N., Hasezawa, S., 2010. Quantification and cluster analysis of actin cytoskeletal structures in plant cells: role of actin bundling in stomatal movement during diurnal cycles in Arabidopsis guard cells. Plant J. 61 (1), 156–165. https://doi.org/10.1111/j.1365-313X.2009.04032.x.

Holowenko, F.M., Mackinnon, M.D., Fedorak, P.M., 2002. Characterization of napthenic acids in oil sands wastewaters by gas chromatography-mass spectrometry. Water Res. 36, 2843–2855 (http://doi.org/S0043-1354(01)00492-4 [pii]).

Jaipargas, E.-A., Mathur, N., Bou Daher, F., Wasteneys, G.O., Mathur, J., 2016. High light intensity leads to increased peroxule-mitochondria interactions in plants. Front. Cell Dev. Biol. 4, 1–11. https://doi.org/10.3389/fcell.2016.00006.

Kamaluddin, M., Zwiazek, J.J., 2002. Naphthenic acids inhibit root water transport, gas exchange and leaf growth in aspen (Populus tremuloides) seedlings. Tree Physiol. 22, 1265–1270. https://doi.org/10.1093/treephys/22.17.1265.

Lee, H.Y., Back, K., 2017. Cadmium disrupts subcellular organelles, including chloroplasts, resulting in melatonin induction in plants. Molecules 22 (10). https://doi.org/10.3390/molecules22101791.

Leishman, C., Widdup, E.E., Quesnel, D.M., Chua, G., Gieg, L.M., Samuel, M.A., Muench, D.G., 2013. The effect of oil sands process-affected water and naphthenic acids on the germination and development of Arabidopsis. Chemosphere 93 (2), 380–387. https://doi.org/10.1016/j.chemosphere.2013.04.101.

Li, C., Fu, L., Stafford, J., Belosevic, M., Gamal El-Din, M., 2017. The toxicity of oil sands process-affected water (OSPW): a critical review. Sci. Total Environ. 601–602, 1785–1802. https://doi.org/10.1016/j.scitotenv.2017.06.024.

Livanos, P., Galatis, B., Apostolakos, P., 2014. The interplay between ROS and tubulin cytoskeleton in plants. Plant Signal. Behav. 9 (1), e28069. https://doi.org/10.4161/psb.28069.

Mathur, J., Mammone, A., Barton, K.A., 2012. Organelle extensions in plant cells. J. Integr. Plant Biol. 54 (11), 851–867. https://doi.org/10.1111/j.1744-7909.2012.01175.x.

McFarlane, H.E., Döring, A., Persson, S., 2014. The cell biology of cellulose synthesis. Annu. Rev. Plant Biol. 65, 69–94. https://doi.org/10.1146/annurev-arplant-050213-040240.

McKenna, J.F., Webb, S.E.D., Kriechbaumer, V., Hawes, C., 2018. Is actin filament sliding responsible for endoplasmic reticulum and Golgi movement? BioRxiv, pp. 1–26 https://doi.org/10.1101/347187

Meijering, E., Dzyubachyk, O., Smal, I., 2012. Methods for cell and particle tracking. Methods Enzymol. 504 (9), 183–200. https://doi.org/10.1016/B978-0-12-391857-4.00009-4.

Morandi, G.D., Wiseman, S.B., Pereira, A., Mankidy, R., Gault, I.G.M., Martin, J.W., Giesy, J.P., 2015. Effects-directed analysis of dissolved organic compounds in oil sands process-affected water. Environ. Sci. Technol. 49 (20), 12395–12404. https://doi.org/10.1021/acs.est.5b02586.

Morandi, G.D., Wiseman, S.B., Guan, M., Zhang, X.W., Martin, J.W., Giesy, J.P., 2017. Elucidating mechanisms of toxic action of dissolved organic chemicals in oil sands process-affected water (OSPW). Chemosphere 186, 893–900. https://doi.org/10.1016/j.chemosphere.2017.08.025.

Nebenführ, A., Dixit, R., 2018. Kinesins and myosins: molecular motors that coordinate cellular functions in plants. Annu. Rev. Plant Biol. 69, 329–361. https://doi.org/10.1146/annurev-arplant-042817.

Nebenführ, A., Gallagher, L.A., Dunahay, T.G., Frohlick, J.A., Mazurkiewicz, A.M., Meehl, J.B., Staehelin, L.A., 1999. Stop-and-go movements of plant Golgi stacks are mediated by the acto-myosin system. Plant Physiol. 121, 1127–1142. https://doi.org/10.1104/pp.121.4.1127.

Nelson, B.K., Cai, X., Nebenführ, A., 2007. A multicolored set of in vivo organelle markers for co-localization studies in Arabidopsis and other plants. Plant J. 51 (6), 1126–1136. https://doi.org/10.1111/j.1365-313X.2007.03212.x.

Nick, P., 2013. Microtubules, signalling and abiotic stress. Plant J. 75 (2), 309–323. https://doi.org/10.1111/tpj.12102.

Paredez, A.R., Somerville, C.R., Ehrhardt, D.W., 2006. Visualization of cellulose synthase demonstrates functional association with microtubules. Science 312, 1491–1496.

Pavlović, K., Grbović, L., Vasiljević, B., Župunski, A., Putnik-Delić, M., Maksimović, I., Kevrešan, S., 2015. The influence of naphthenic acids and their fractions on cell membrane permeability. J. Serb. Chem. Soc. 80 (6), 749–754. https://doi.org/10.2298/JSC141201012P.

Protić, M., Sabljić, A., 1989. Quantitative structure-activity relationships of acute toxicity of commercial chemicals on fathead minnows: effect of molecular size. Aquat. Toxicol. 14 (1), 47–64. https://doi.org/10.1016/0166-445X(89)90054-4.

Rowland, S.J., Scarlett, A.G., Jones, D., West, C.E., Frank, R.A., 2011. Diamonds in the Rough: Identification of Individual Naphthenic Acids in Oil Sands Process Water. Environ. Sci. Technol. 45, 3154–3159. https://doi.org/10.1021/es103721b.

Rudolph-Mohr, N., Vontobel, P., Oswald, S.E., 2014. A multi-imaging approach to study the root-soil interface. Ann. Bot. 114 (8), 1779–1787. https://doi.org/10.1093/aob/mcu200.

Satiat-Jeunemaitre, B., Steele, C., Hawes, C., 1996. Golgi-membrane dynamics are cytoskeleton dependent: a study on Golgi stack movement induced by brefeldin a. Protoplasma 191, 21–33.

Schindelin, J., Arganda-Carreras, I., Frise, E., Kaynig, V., Longair, M., Pietzsch, T., ... Cardona, A., 2012. Fiji: an open-source platform for biological-image analysis. Nat. Methods 9 (7), 676–682. https://doi.org/10.1038/nmeth.2019.

Schultz, T., 1989. Nonpolar narcosis: a review of the mechanism of action for baseline aquatic toxicity. Aquatic Toxicology and Hazard Assessment, 12th ed. ASTM International, West Conshohocken, PA, pp. 104–109.

Schwarzerová, K., Zelenková, S., Nick, P., Opatrný, Z., 2002. Aluminum-induced rapid changes in the microtubular cytoskeleton of tobacco cell lines. Plant Cell Physiol. 43 (2), 207–216. https://doi.org/10.1093/pcp/pcf028.

Scott, A., Wyatt, S., Tsou, P.L., Robertson, D., Stromgren Allen, N., 1999. Model system for plant cell biology: GFP imaging in living onion epidermal cells. BioTechniques 26 (6), 1125–1152.

Scuffi, D., Nietzel, T., Di Fino, L., Meyer, A.J., Lamattina, L., Schwarzländer, M., ... Garcia-Mata, C., 2018. Hydrogen sulfide increases production of NADPH oxidase-dependent hydrogen peroxide and phospholipase D-derived phosphatidic acid in guard cell signaling. Plant Physiol. 176, 2532–2542. https://doi.org/10.1104/pp.17.01636.

Sinclair, A.M., Trobacher, C.P., Mathur, N., Greenwood, J.S., Mathur, J., 2009. Peroxule extension over ER-defined paths constitutes a rapid subcellular response to hydroxyl stress. Plant J. 59 (2), 231–242. https://doi.org/10.1111/j.1365-313X.2009.03863.x.

Small, C.C., Cho, S., Hashisho, Z., Ulrich, A.C., 2015. Emissions from oil sands tailings ponds: review of tailings pond parameters and emission estimates. J. Pet. Sci. Eng. 127, 490–501. https://doi.org/10.1016/j.petrol.2014.11.020.

Sun, J., Peng, H., Alharbi, H.A., Jones, P.D., Giesy, J.P., Wiseman, S.B., 2017. Identification of chemicals that cause oxidative stress in Oil Sands process-affected water. Environ. Sci. Technol. 51 (15), 8773–8781. https://doi.org/10.1021/acs.est.7b01987.

Tollefsen, K.E., Petersen, K., Rowland, S.J., 2012. Toxicity of synthetic naphthenic acids and mixtures of these to fish liver cells. Environ. Sci. Technol. 46 (9), 5143–5150. https://doi.org/10.1021/es204124w.

Van Gestel, K., Köhler, R.H., Verbelen, J.-P., 2002. Plant mitochondria move on F-actin, but their positioning in the cortical cytoplasm depends on both F-actin and microtubules. J. Exp. Bot. 53 (369), 659–667. https://doi.org/10.1093/jexbot/53.369.659.

Waszczak, C., Carmody, M., Kangasjärvi, J., 2018. Reactive oxygen species in plant signaling. Annu. Rev. Plant Biol. 69, 209–236. https://doi.org/10.1007/978-3-642-00390-5.

Whitby, C., 2010. Advances in applied microbiology. Microbial Naphthenic Acid Degradation, 1st ed. vol. 70. Elsevier Inc.. https://doi.org/10.1016/S0065-2164(10)70003-4.

Whittington, A.T., Vugrek, O., Wei, K.J., Hasenbein, N.G., Sugimoto, K., Rashbrooke, M.C., Wasteneys, G.O., 2001. MOR1 is essential for organizing cortical microtubules in plants. Nature 411 (6837), 610–613. https://doi.org/10.1038/35079128.

Widdup, E.E., Chatfield-Reed, K., Henry, D., Chua, G., Samuel, M.A., Muench, D.G., 2015. Identification of detoxification pathways in plants that are regulated in response to treatment with organic compounds isolated from oil sands process-affected water. Chemosphere 139, 47–53. https://doi.org/10.1016/j.chemosphere.2015.05.048.

Wiseman, S.B., Anderson, J.C., Liber, K., Giesy, J.P., 2013. Endocrine disruption and oxidative stress in larvae of Chironomus dilutus following short-term exposure to fresh or aged oil sands process-affected water. Aquat. Toxicol. 142–143, 414–421. https://doi.org/10.1016/j.aquatox.2013.09.003.

Yoshinaga, K., Arimura, S.I., Niwa, Y., Tsutsumi, N., Uchimiya, H., Kawai-Yamada, M., 2005. Mitochondrial behaviour in the early stages of ROS stress leading to cell death in Arabidopsis thaliana. Ann. Bot. 96 (2), 337–342. https://doi.org/10.1093/aob/mci181.

Zhang, K., Wiseman, S., Giesy, J.P., Martin, J.W., 2016. Bioconcentration of dissolved organic compounds from Oil Sands process-affected water by Medaka (*Oryzias latipes*): importance of partitioning to phospholipids. Environ. Sci. Technol. 50 (12), 6574–6582. https://doi.org/10.1021/acs.est.6b01354.